Deformation and failure in cellular materials

Anthony J. C. Ladd and John H. Kinney
Lawrence Livermore National Laboratory, Livermore, California 94550

Thomas M. Breunig
University of California San Francisco, San Francisco, California 94143

(Received 1 July 1996)

An isotropic, three-dimensional, lattice-spring model is proposed to describe deformation and failure in heterogeneous materials. Young's moduli of samples of trabecular bone have been calculated, using images of the microstructure obtained from x-ray microtomography. An analysis of the stress distribution indicates that trabecular bone will most likely fail due to local tensile stresses, even when the macroscopic load is compressive. In the samples studied, there does not seem to be a homogenization length scale beyond which the material can be described by an effective medium theory. [S1063-651X(97)09703-1]

PACS number(s): 87.45.−k, 62.20.Dc, 81.40.Jj, 82.20.Wt

Trabecular bone is mineralized tissue with an open-cell structure (see Fig. 1) that lies inside the cortical shell. It is known that osteoporosis is strongly correlated with the loss of trabecular bone mass [1], but effective treatment requires an understanding of how the increased fracture risk in osteoporotic patients is related to changes in bone architecture, and to what extent it may be due to changes in mechanical properties of the bone tissue itself. Experimental measurements of the elastic moduli of trabecular bone show a variety of density scalings, depending on the anatomical location and species from which the sample is taken [1]. Thus the mechanical properties of trabecular bone do not follow the simple scaling laws of many *regular* cellular structures [2], nor do they follow the typical scaling laws of random networks [3]. Cellular structures, even irregular ones, are much more highly ordered than random networks; for instance, trabecular bone is mechanically stable even though it is 85–90 % pore space. Separating the effects of architecture and tissue properties on bone biomechanics requires a detailed knowledge of the distribution of stress in *individual* samples where the structure can be accurately determined, for instance by x-ray microtomography [4]. In this paper we describe a numerical simulation technique that can be used to determine the stress and strain fields in complex heterogeneous materials, assuming that on the *microscopic* scale (typically of the order of 1 μm) deformation can be described by the equations of isotropic linear elasticity. Given the stress field throughout the sample and a local failure criteria, the failure process can be determined by successive relaxation of the displacement field. The algorithm is based on a lattice model of the material; the nodes are connected by springs whose force constants are determined by the elastic stiffness of each volume element. It was found by analogy with lattice-gas models [5] that a locally isotropic spring network can be constructed by a suitable mixture of two different sets of connections. An averaging procedure for the force constants at material interfaces is described which substantially improves the convergence of the model.

Consider a cubic lattice, interconnected by springs and described by the Hamiltonian

$$\mathbf{H}=\sum_i \frac{p_i^2}{2m}+\frac{\kappa}{2}\sum_{i>j} g_{ij}[(\mathbf{u}_i-\mathbf{u}_j)\cdot\hat{\mathbf{x}}_{ij}]^2; \tag{1}$$

$\mathbf{u}_i$ is the diplacement of the ith node, and $\mathbf{x}_{ij}=\mathbf{x}_i-\mathbf{x}_j$ is the vector connecting nodes i and j in the undistorted lattice. The force constant κ sets the frequency range of the spring network and the coupling constants g_{ij} are chosen to ensure local isotropy. Although a cubic lattice has insufficient symmetry to ensure elastic isotropy [5], there are simple models that can be used, in conjunction with appropriate choices of coupling parameters g_{ij}, to obtain isotropic elastic equations. The simplest model which is both isotropic and mechanically stable at the element level has 18 different connections, corresponding to the [100] and [110] directions of a cubic lattice; isotropy requires that $g_{ij}=1$ for both [100] and [110] orientations of the vector $\mathbf{x}_{ij}$. Macroscopic field equations can be obtained by a Taylor expansion of the displacements; the resulting elastodynamic equations are correct to second order in the lattice spacing, i.e.,

$$\rho\partial_t^2\mathbf{u}=\frac{\kappa}{a}[2\nabla(\nabla\cdot\mathbf{u})+\nabla^2\mathbf{u}+O(a^2\nabla^4\mathbf{u})]. \tag{2}$$

For central forces the Lamé constants are equal, and Poisson's ratio is therefore $\frac{1}{4}$.

Samples of trabecular bone were imaged in an x-ray tomographic microscope [4], with a resolution of 20 μm (see Fig. 1). A digitized image of each specimen was used to construct a three-dimensional array of cubic volume elements, typically about 30 μm on a side; each volume element was either occupied, signifying bone, or unoccupied, signifying vacuum. In this work it was assumed that the tissue properties are spatially invariant, and that all the spatial inhomogeneity comes from variations in architecture. In order to set up a spring network for a particular trabecular microstructure, we imagine that each *occupied* volume element (or voxel) of the tomographic image (see Fig. 1) is represented by one or more elastic elements in the model; a cross section through a typical strut contains 10–100 voxels. Nodes are placed at the vertexes of each elastic element and

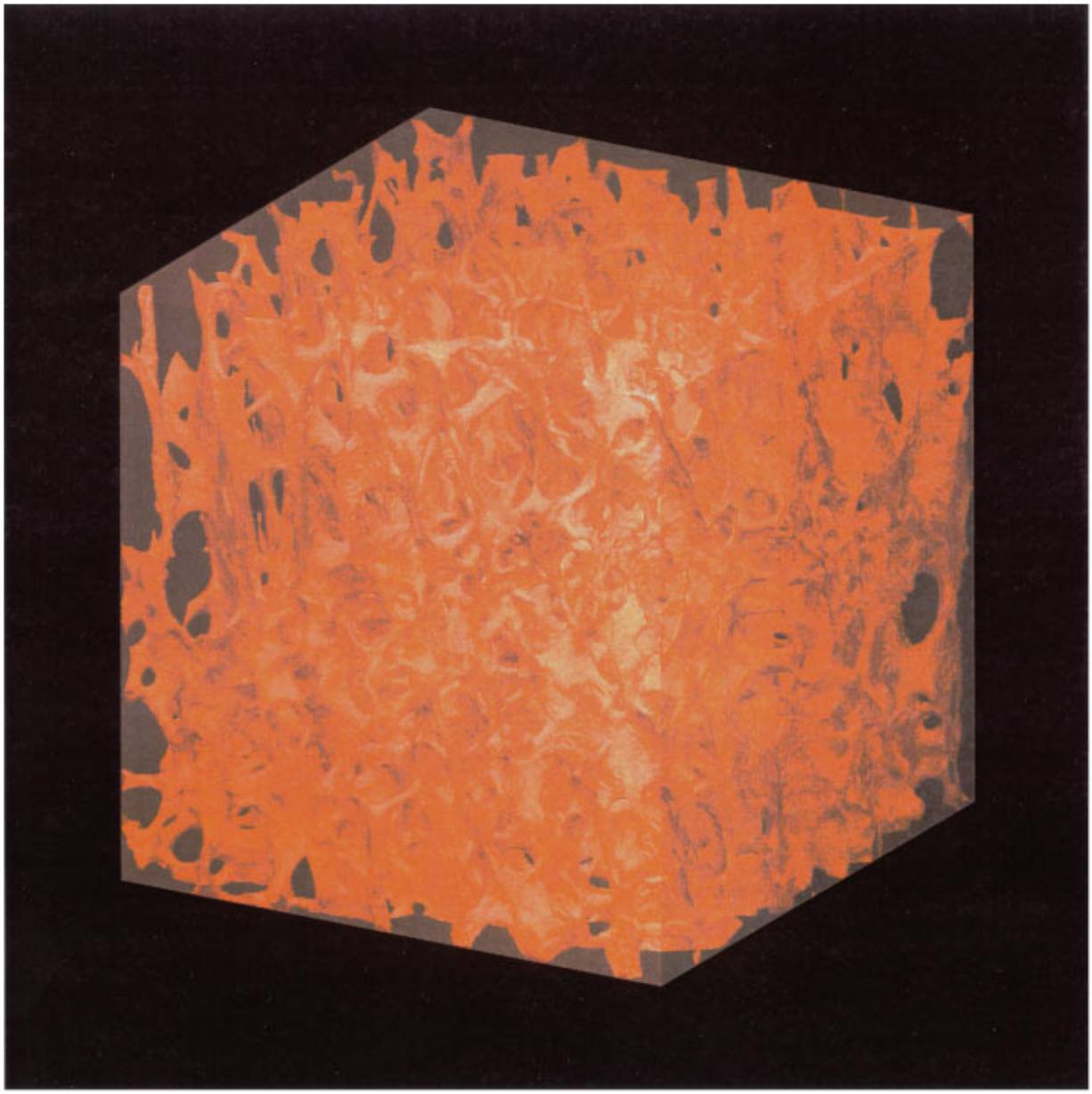

FIG. 1. (Color) X-ray tomographic image of a sample of trabecular bone at a resolution of 20 μm; the sample is about 7 mm on a side, or about 350 voxels. The structure is largely composed of interconnected struts and plates; these are typically about 100 μm thick. The proximal-distal (longitudinal) direction corresponds to the vertical direction in the figure, the medial-lateral axis runs from front to back, and the dorsal-palmer axis runs right to left. The sample porosity is about 86%. Figures 1 and 3 may be viewed at http://www-ep.es.llnl.gov/www-ep/esd/shockphy/bonemech.html.

interconnected by springs; this spring network fills 10–15 % of the total volume. Each elastic element is assumed to contribute to the force constant of the springs associated with that element. Thus element i contributes $\frac{1}{4}\kappa_i$ to each of the 12 surrounding [100] springs, where κ_i characterizes the bulk stiffness of the material in element i. The total force constant of a [100] spring is made up of contributions from up to four surrounding elements. In the interior of the solid the spring constant will be that of the bulk material κ, but near an interface it will be weighted by the material properties of the adjoining elements, taking κ_i to be zero for unoccupied voxels. Similarly, an element contributes $\frac{1}{2}\kappa_i$ to each of its 12 [110] springs, which are shared between two neighboring volume elements. The resulting spring network is mechanically stable for any architecture, as long as the structure is a continuous, face-connected cluster. Although this model is more complex to set up than a simple spring model [3], it leads to a much more rapid convergence as the number of voxels is increased. For example, consider a uniform bar with a square cross section; if a spring model with a single force constant is used, then it is found that the calculated Young's modulus deviates from continuum theory by terms proportional to $1/h$, where h is the number of voxels on a side of the square. However, weakening the surface springs, as described above, gives an h-independent Young's modulus, equal to the continuum result for the same bulk force constant.

Spring network models typically incorporate failure by

TABLE I. Elastic constants of two samples of human trabecular bone. The compressional moduli for uniaxial loadings E_i are normalized by Young's modulus for the bulk material E_0. The elastic anisotropies $\beta_2 = E_2/E_1$ and $\beta_3 = E_3/E_1$ are also shown, together with experimental data from Ref. [6]. By combining experimental and simulation data for longitudinal loading, an estimate of the Young's modulus of the tissue material, E_0, is obtained.

Sample	Porosity	E_1/E_0	E_2/E_0	E_3/E_0	β_2	β_3	E_0 (GPa)
1	87%	0.0374	0.0182	0.0136	0.49	0.36	
Expt.					0.47	0.73	12
2	86%	0.0513	0.0171	0.0165	0.33	0.32	
Expt.					0.37	0.14	12

breaking individual springs in response to large local extensions [3]. While this is physically appealing, experimental failure measurements are usually described in terms of principal stress or strain energy, which are only indirectly related to the stretching of individual bonds. We propose to model failure at the element level, rather than at the level of the individual springs. First the strain in each element is calculated, using an expression for the symmetric strain tensor $\boldsymbol{\epsilon}^s$ appropriate to cubic elements,

$$\boldsymbol{\epsilon}^s = \frac{1}{4a^2}\sum_{i=1}^{8} (\mathbf{x}_i\mathbf{u}_i + \mathbf{u}_i\mathbf{x}_i); \tag{3}$$

here $\mathbf{x}_i$ is the vector from the center of the element to the vertex i. It can then be determined by continuum elasticity whether or not the element has failed, under the chosen failure criterion. If an element is found to have failed, its contributions to the surrounding spring constants are removed and the displacements are again relaxed.

Trabecular bone is structurally and elastically anisotropic (see Fig. 1). In the distal radius the preferred direction lies along the main axis of the forearm, the longitudinal (proximal-distal) direction. The trabeculae are randomly oriented about the longitudinal axis; thus the bone is roughly isotropic in the two transverse directions (medial-lateral and dorsal-palmer). In Table I we report calculated elastic constants for two samples of human trabecular bone. Constant-displacement boundary conditions were used along the compression direction, with the lateral displacements on the compressional surfaces constrained to zero; the displacements on the unloaded surfaces were free. These boundary conditions are thought to represent most realistically the experimental situation, where the sample is firmly gripped between the load platens. The displacement field was relaxed, using a conjugate-gradient algorithm, until the change in potential energy was less than one part in 10^{12}. The data in Table I were obtained with cubic elastic elements that were 30–40 μm on a side. Some of the calculations were repeated with twice as many elements in each dimension; about a 3% variation in the moduli was found.

The calculated Young's moduli for these samples range from 1% to 5% of the Young's modulus for the bulk material (Table I). Since experimental measurements of the tissue modulus are not yet available, we compare ratios of elastic moduli in different directions. The two transverse-longitudinal anisotropies β_2 and β_3 are compared with experimental measurements [6] on the same samples. The results for the first anisotropy (medial-lateral–proximal-distal), β_2, are in good agreement with experimental data. However the agreement between simulation and experiment for the second anisotropy (dorsal-palmer–proximal-distal), β_3, is poor; we think this is due to sample damage during the experimental measurements. Since the dorsal-palmer modulus was always measured last, trabeculae near the surfaces may have been broken during the repeated loading and unloading cycles that were used for the stress-strain measurements in the other directions.

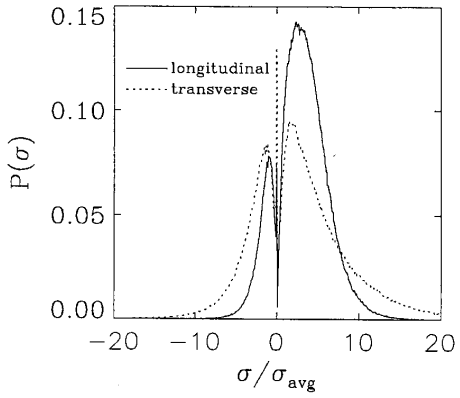

FIG. 2. Stress histograms for sample 2. The probability distribution of the largest principal stress is shown for longitudinal and transverse compressive loadings. The stresses are normalized by the mean stress in the sample; the area under each curve is unity.

A rough estimate of the tissue modulus has been made by combining the experimental measurement of the longitudinal (proximal-distal) modulus, E_1 [6], with the simulation data for the ratio of longitudinal modulus to tissue modulus E_1/E_0. The longitudinal modulus was used because we believe this is the most reliable experimental measurement. We estimate that the tissue modulus for both samples is about 12 GPa, at the upper end of the published range of values for trabecular bone (1–15 GPa) [1].

Histograms of the largest principal stress are shown in Fig. 2, for longitudinal and transverse loadings. It can be seen that the largest stress on an element can be either compressive ($\sigma/\sigma_{\text{avg}} > 0$) or tensile ($\sigma/\sigma_{\text{avg}} < 0$). Even though the samples are macroscopically loaded in compression, there are a substantial number of elements ($\approx 25\%$) that are in tension. Failure is expected to begin at the elements with the highest tensile stresses. This is in agreement with experimental data [7], which indicate that trabecular bone fails by breaking struts (tensile failure) rather than by plastic yielding (shear failure). There is a pronounced difference in the widths of the two distributions; under transverse loading the sample has a larger fraction of highly stressed elements than when loaded in the longitudinal direction. This is because longitudinal loading deforms the main trabecular loops, whereas transverse loading tends to bend the more fragile connections between trabeculae. Thus the bone is more likely to fail under transverse loading than principal-axis loading.

Three-dimensional images of the largest principal stress are shown in Fig. 3, for longitudinal and transverse loadings. In each image, the elements whose stress exceeds a preset

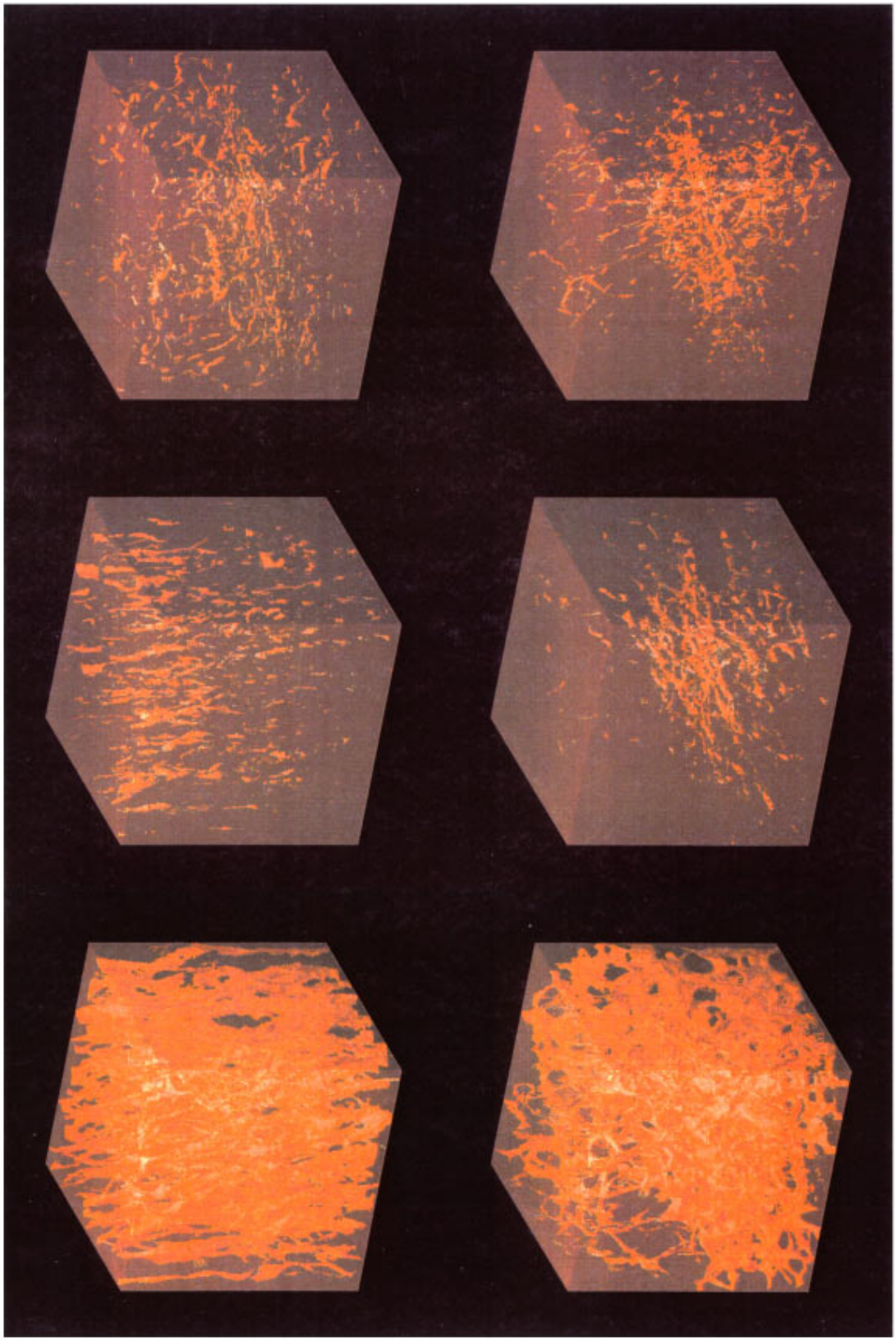

FIG. 3. (Color) Distribution of load paths in sample 2. The upper three images show compressive loading along the proximal-distal axis (bottom to top); the lower three images show compressive loading along the medial-lateral axis (front to back). The elements where the largest principal stress exceeds a preset level are illuminated; the variation in brightness is only to enhance the perspective. The stress levels were set so that a specific fraction of elements are shown in each image. The moderate compression images (left) contain 50% of the occupied voxels; the high compression images (center) and high tension images (right) each contain 5% of the occupied voxels.

value are illuminated; images are shown at three different stress levels, corresponding to moderate compression, high compression, and high tension, respectively. At the lowest stress level (upper-left and lower-left images) the load paths clearly outline the trabecular structure, as can be seen by comparison with Fig. 1. At higher stress levels (center images), the load paths are fewer and are distributed inhomogeneously; the orientations of the load paths are readily identifiable. It has been assumed, based on two-dimensional observations of the architecture [8], that trabecular bone is homogeneous on length scales longer than a few trabecular spans. Our results show that the stress is not homogenized until much larger length scales, if at all. Tensile stresses (upper-right and lower-right images) are typically located on the outside of curved struts, as can be seen by comparing these images with the structure shown in Fig. 1. There is a concentration of tension near the center of the sample, where thicker trabeculae begin to distribute the load more uniformly. These images show how relatively minor variations in architecture can have a substantial impact on the stress distribution in irregular cellular structures; the location of regions of stress concentration vary considerably with load direction.

In this paper we have described an approach to solving problems involving deformation of complex, cellular solids; we found that it was feasible to simulate structures containing up to 10^7 nodes on a workstation. By a careful choice of spring constants, a more quantitative connection to continuum elasticity is possible than with the simpler spring models typically used to analyze random networks [3]. Analysis of the stress distribution in samples of trabecular bone shows that tensile failure is the likely mode of failure, even when the samples are loaded in compression. Our calculations also indicate that the stress field is not homogeneous until rather large length scales, if at all; this suggests that effective medium theories, which ignore the local microstructure, will be unable to describe failure in trabecular bone.

This work was supported by the the National Institutes of Health (R01-AR43052), by the U. S. Department of Energy Office of Basic Energy Sciences (KC040301), and by Lawrence Livermore National Laboratory under Contract No. W-7405-Eng-48.

[1] T. M. Keaveny and W. C. Hayes, J. Biomech. **27**, 1127 (1993).
[2] L. J. Gibson, Mater. Sci. Eng. A **110**, 1 (1989).
[3] H. J. Herrman and S. Roux, *Statistical Models for the Fracture of Disordered Materials* (North-Holland, Amsterdam, 1990).
[4] J. Kinney *et al.*, Science **260**, 789 (1993).
[5] U. Frisch *et al.*, Complex Systems **1**, 649 (1987).
[6] S. Majumdar *et al.*, Osteoporosis Int. **6**, 376 (1996).
[7] T. M. Keaveny *et al.*, J. Biomech. Eng. **115**, 534 (1994).
[8] T. P. Harrigan, M. Jasty, R. W. Mann, and W. H. Harris, J. Biomech. **21**, 269 (1988).